Layup Strategies for in-situ Automated Fiber Placement of Complex Geometries

Lukas Raps[1], Ashley R. Chadwick[1], Heinz F. Voggenreiter[1]
[1]German Aerospace Center (DLR) - Institute of Structures and Design, Pfaffenwaldring 38-40, 70569 Stuttgart, Germany

ABSTRACT

With meticulous process control and the correct manufacturing parameters, competitive mechanical properties have been achieved using in-situ Automated Fiber Placement (AFP). Complex geometries, particularly double curvatures required for real part geometries, however, present additional obstacles to the already challenging process. Without post-consolidation in a hot press or autoclave, the severity of geometry-related deviations from the ideal ply composition, namely fiber steering defects, gaps or overlaps, remains unquantified. Variable Stiffness Panels can be used as a two-dimensional representation of double-curved geometries, since the curved layup paths result in the same kind of defects. This work suggests optimized layup strategies for constant curvature Variable Stiffness Panels considering in-situ AFP process characteristics and limitations. The correlations between layup strategy parameters and the resulting layup deviations is analyzed, providing algorithms for optimized layup strategies for in-situ AFP on complex geometries.

1. Introduction

In-situ Automated Fiber Placement has great potential to reduce manufacturing costs and time by combining the additive manufacturing and consolidation processes into one single process and omitting subsequent autoclave- or press consolidation process steps. However, without subsequent bulk consolidation, defects which inevitable arise from complex geometries inevitably end up in the final laminate as they cannot be mitigated in an autoclave or press consolidation process. Variable Stiffness Panels are suitable as a two-dimensional representation of complex geometries, since the same geometry-related defects such as gaps and overlaps or steering defects following high in-plane path curvature occur due to their stiffness-optimized curved paths. Layup strategies optimized for the characteristics of the in-situ AFP manufacturing process are suggested in this work. A parametric Python script for constant curvature Variable Stiffness Panels was developed based on analytical functions, allowing for an exact calculation of defect sizes for a wide range of input variables. Based on the Python algorithm, a parameter study was carried out to demonstrate the correlations between layup strategy and resulting defects and to find Variable Stiffness Panel configurations suitable for the in-situ AFP process.

1.1. Layup strategies

A layup strategy for a complex surface is defined by an initial reference curve and a method for generating subsequent paths. Two main aspects are therefore addressed: the choice of reference curve and the propagation of the paths. The reference curve originates from a starting point and determines the fiber orientation along the first course. Rousseau et al. [34] categorized reference curves into fixed angle, geodesic and variable angle reference curves. Fixed-angle reference curves (rosette rule) keep the local fiber angle constant with respect to a global coordinate system. No fiber angle deviation occurs, but severe steering can arise for highly curved geometries. Geodesic reference curves are defined as paths without in-plane curvature and thus avoid steering but may introduce angle deviation [8]. Variable angle reference curves exploit steering capabilities of AFP technolgy to optimize stiffness properties of composite laminates. Gürdal et al. demonstrated significant stiffness improvements of Variable Stiffness Panels compared to standard composite panels [14, 35, 15, 22, 23] and Blom et al. employed the Variable Stiffness concept for cylindrical and conical geometries [3, 7, 6, 4, 5]. Variable angle reference curves can again be divided into different categories. Constant curvature reference curves are used most frequently. A parametric definition of constant curvature reference curves for a surface $S(u, v)$ and geodesic curvature K_g is presented in [34]:

$$\begin{aligned} u'' + \Gamma^1_{11}u'^2 + 2\Gamma^1_{12}u'v' + \Gamma^1_{22}v'^2 &= \frac{k_g(Fu' + Gv')\sqrt{Eu'^2 + 2Fu'v' + Gv'^2}}{\sqrt{EG - F^2}} \\ v'' + \Gamma^2_{11}u'^2 + 2\Gamma^2_{12}u'v' + \Gamma^2_{22}v'^2 &= \frac{-k_g(Eu' + Fv')\sqrt{Eu'^2 + 2Fu'v' + Gv'^2}}{\sqrt{EG - F^2}} \end{aligned} \tag{1}$$

where E, F and G are the fundamental coefficients of the surface $S(u, v)$, defined as

$$\begin{aligned} E(u, v) &= \frac{\partial S}{\partial u} \cdot \frac{\partial S}{\partial u} \\ F(u, v) &= \frac{\partial S}{\partial u} \cdot \frac{\partial S}{\partial v} \\ G(u, v) &= \frac{\partial S}{\partial v} \cdot \frac{\partial S}{\partial v} \end{aligned} \tag{2}$$

The differential equation system can be simplified for flat laminates:

$$\begin{aligned} x(t) &= x_0 + \frac{1}{K}\cos(t) \\ y(t) &= y_0 + \frac{1}{K}\sin(t) \end{aligned} \tag{3}$$

where the curvature $K = K_g$ as the normal curvature of a flat surface is 0. For flat panels, constant curvature variable stiffness reference curves were investigated in [15, 6, 29, 11].

After the first course, subsequent courses are generated by either parallel path propagation, which offsets the reference curve perpendicularly along the surface, or shifted path propagation, which translates the entire curve without changing its steering radius. Parallel propagation yields gap-free layups but can lead to severe steering radii and angle deviation on curved surfaces, whereas shifted propagation preserves steering but may introduce overlap or gap defects [15, 20].

1.2. Variable Stiffness Panels

Variable stiffness panels exploit tailored fiber orientations to enhance structural performance, yielding significant gains in stiffness, buckling resistance, and post-buckling stiffness [33]. Numerous studies have developed analytical and numerical design frameworks for Variable Stiffness Panels [14, 15, 22, 16, 21, 2, 4, 10, 18, 38, 30, 17, 28], with a comprehensive review in [13]. Manufacturing constraints such as steering- and gap/overlap defects are inherent to the curved fiber paths, particularly for thermoset AFP processes [15, 6, 1, 29, 10, 24, 39, 36]. Incorporating a steering-radius limit reduced the buckling-load benefit from 111 % to 57 % relative to a conventional laminate [11]. A defect-layer approach accurately modeled gaps/overlaps; with overlaps the buckling-load improvement rises to 105 % versus 56 % without them, while a full-gap design yields only 40 % load increase [12, 11, 27]. Wider prepreg tape exacerbates triangular gaps, lowering strength [12].

Experimental validation of thermoset AFP Variable Stiffness Panels confirmed these trends. Marouene et al. [26, 25] reported 45 % and 22 % higher weight-normalized buckling loads for 0 % (gaps) and 100 % (overlaps) coverage-ratio panels, respectively, versus a quasi-isotropic reference. Khani et al. [19] obtained an 85 % higher ultimate load in a tensile test of an optimized Variable Stiffness Panel with a central cut-out, surpassing both a quasi-isotropic and a straight-fiber optimized laminate. Zhu et al. [40] found a 36 % improvement for a similar configuration, while Peeters et al. [31] achieved 11.7 % higher buckling load and 15 % weight savings with a 50 % coverage-ratio Variable Stiffness Panel. To date, however, thermoplastic Variable Stiffness Panels and in-situ AFP manufacturing signatures remain unexplored.

2. Methodology

Based on the state of the art design methodology for constant curvature Variable Stiffness Panels [11], an analytical Python path planning script was developed, considering the in-situ AFP process characteristics. A brief description of the underlying analytical functions is presented below. From the parameterization introduced in Equation 3, the following form can be derived using the trigonometric identity $sin^2(t) + cos^2(t) = 1$:

$$y(x) = \begin{cases} \sqrt{\rho^2 - (x - \rho \cdot cos(T_0))^2} - \rho \cdot sin(T_0) & \text{if } x < 0 \\ -\sqrt{\rho^2 - (x + \rho \cdot cos(T_0))^2} + \rho \cdot sin(T_0) & \text{if } x \geq 0 \end{cases} \tag{4}$$

where T_0 is the angle between the y-axis and the reference curve $y(x)$ at the origin and ρ is the steering radius of the constant curvature reference curve (Figure 1(a)). The angle T_0, steering radius ρ and laminate width w determine the angle T_1 at the lateral boundaries of the laminate. Constant curvature Variable Stiffness Panel designs using this reference path definition were presented in [6, 11]. The first set of parallel tows is defined by the reference curve leading through the coordinate origin. It can be viewed as individual tows placed in parallel or as a course of simultaneously placed tows using a multiple-tape end effector. An example with 16 parallel half-inch tows is presented in Figure 1(b). To keep the local fiber angle constant in relation to the x-coordinate, the reference curve for the

next set of parallel tapes is shifted by the shifting distance D in the y-direction. Tow cuts are required at the intersection of course boundaries to avoid overlaps. One-sided tow cuts at the upper boundary of each course were suggested in the literature [6, 11]. This approach is presented for 0 % coverage (gaps design) in Figure 1(b). This strategy results in three disadvantageous effects for the AFP process. Firstly, both, track starts and track ends are required on the panel. Track ends, however, results in sub-optimum consolidation, since the interface between tape and substrate can no longer be heated after the tape fold-down, when the tape leaves the tape guiding system [32]. Secondly, tape cuts are required at the inside and outside boundary of the steered course. Tow-straightening at outside cuts and resulting deviation from the intended layup path [3, 37], however make this a non-preferable cutting position. Thirdly, this strategy results in very short tows (Figure 1(b)), which can be an issue with the minimum cut length capabilities of the AFP end-effector.

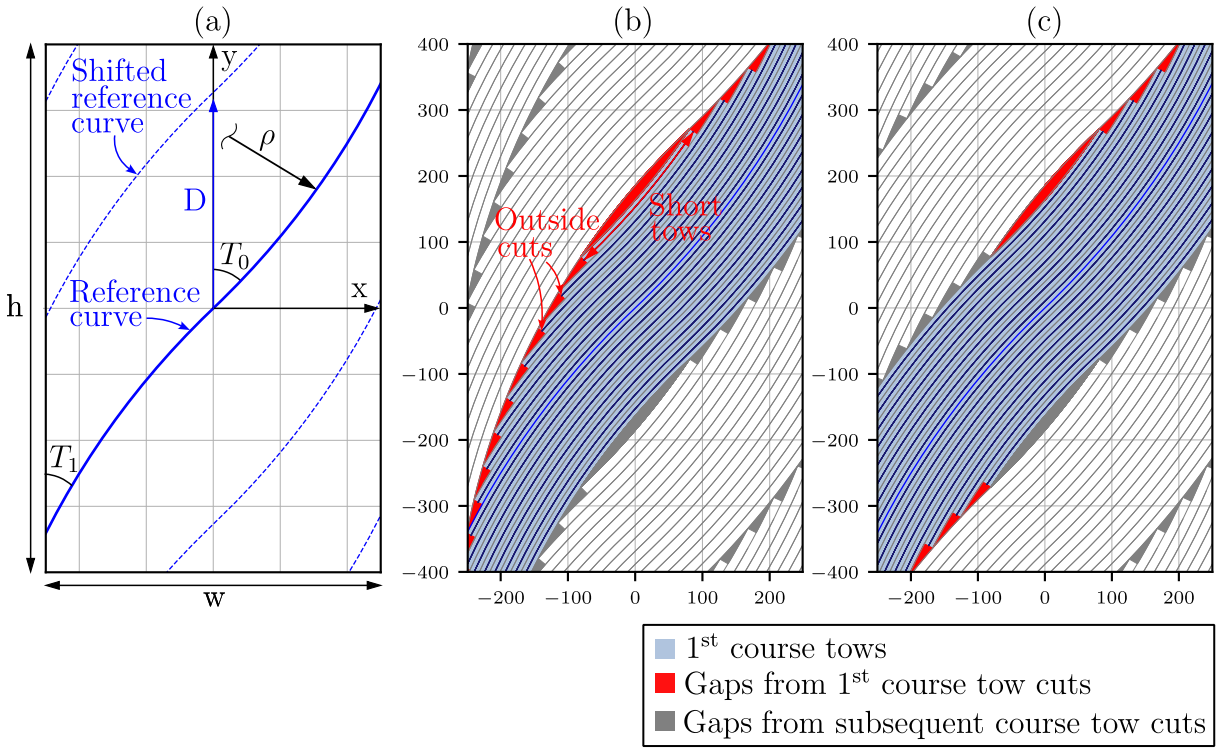

Figure 1: Constant curvature Variable Stiffness Panel design with 0 % coverage ratio: (a) Reference curve definition, (b) One-sided tow cuts [6, 11], (c) Tow cuts on the inside radius of the steered course

To this end, a novel strategy is suggested in this work with tow cuts only at the inside boundary of the steered course (Figure 1(c)). The presented example where, $T_1 < T_0$, tows are therefore cut at the lower boundary of the steered course for $x < 0$ and at the upper boundary for $x > 0$. Tow-straightening, minimum cut length and track ends with sub-optimum consolidation can thus be avoided, resulting in a layup strategy that is advantageous for the in-situ AFP process. The same principle can also be applied to a 100 % coverage ratio (overlaps) design, which is presented in Figure 2.

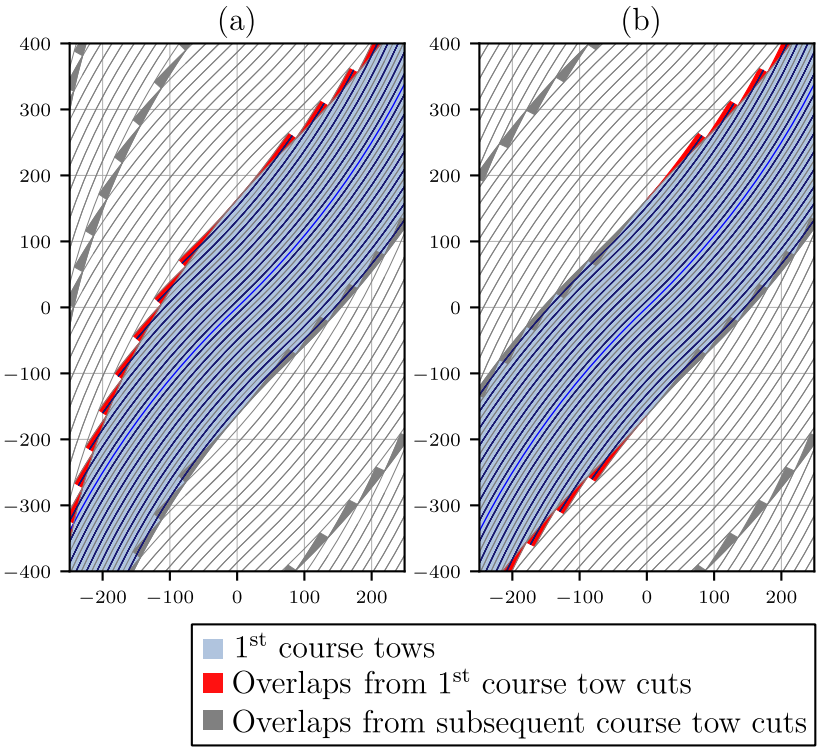

Figure 2: Constant curvature Variable Stiffness Panel design with 100 % coverage ratio: (a) One-sided tow cuts, (b) Tow cuts on the inside radius of the steered course

Based on this design principle, an analytical Python algorithm was developed, that calculates resulting in-plane curvatures, angle deviations and gap or overlap defects for varying reference curves, number of parallel tapes, tape width and other input variables. Figure 3 presents a list of input variables and analysis results. A detailed description of the analytical algorithm is presented in Appendix 1.

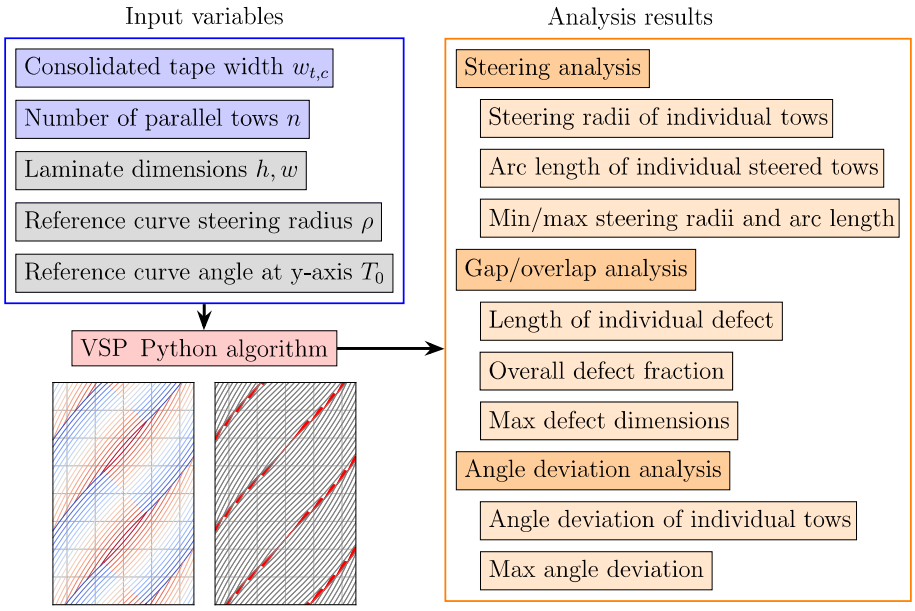

Figure 3: Variable Stiffness Panel Python algorithm - Input parameters and analysis results

The panel dimensions and reference curve geometry are determined by the stiffness optimization of the Variable Stiffness Panel design. The AFP layup strategy-specific parameters tape width and number of parallel tows, on the other hand, are chosen based on manufacturing constraints of the AFP process. A parameter study based on the analytical Python algorithm was therefore carried out for fixed laminate dimensions ($h = 800\ mm$, $w = 500\ mm$) and reference curve geometry ($T_0 = 46$, $\rho = 1250\ mm$) while varying consolidated tape width and the number of parallel tows to compare the resulting angle deviation, steering and gap and overlap defects.

3. Results and Discussion

The impact of the tow cutting strategy on the angle deviation is illustrated in Figure 4. For an example with 16 parallel tows and 14 mm width of individual tows, the heat map plots of the angle deviation show significantly larger angle deviation (a maximum value of 14.1 °) on the left hand side of the one-sided tow cuts plot (Figure 4(a)) compared to the tow cuts at the inside radius (Figure 4(b)), reaching a maximum of 6.6 °. The corresponding parameter plot for varying number of parallel tows and varying width of individual tows is presented in Figure 5. The maximum and average angle deviation is visualized for the respective Variable Stiffness Panels with (a) one-sided tow cuts and (b) tow cuts at the inner radius. An increase in course witdth either by a larger number of parallel tows or wider individual tows results in an increase in maximum angle deviation. A wider course results in a larger distance between the reference curve and the tows at the edges of the course. This leads to a larger angle deviation at the course edges and thus primarily affects the maximum angle deviation values. The average angle deviation, on the other hand, remains at the same level for both tow cut strategies.

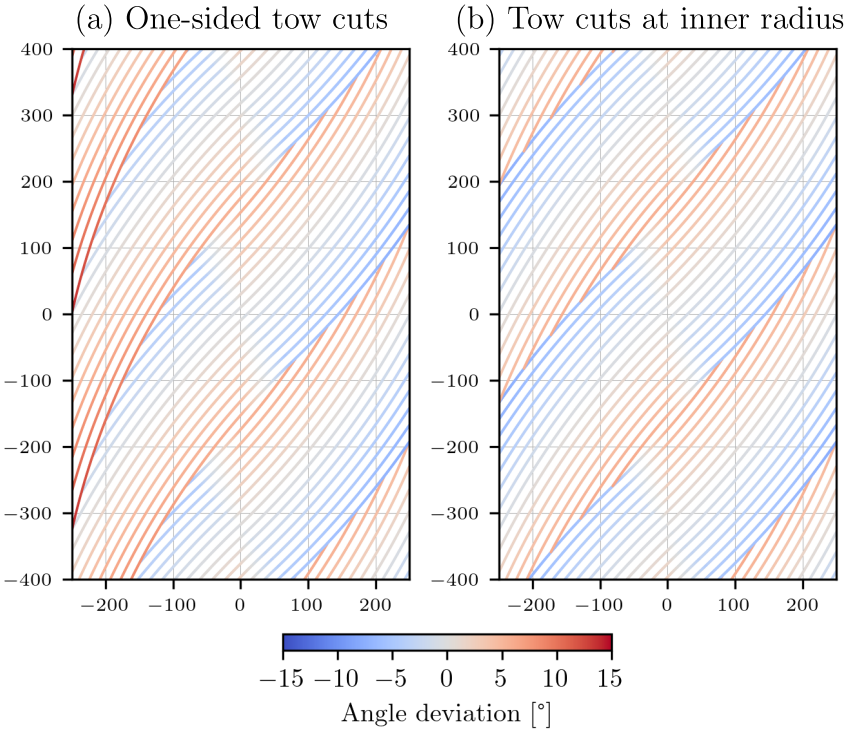

Figure 4: Variable Stiffness Panel angle deviation analysis: (a) One-sided tow cuts, 16 parallel tows, 14 mm width of individual tows (b) Tow cuts at inner radius, 16 parallel tows, 14 mm width of individual tows

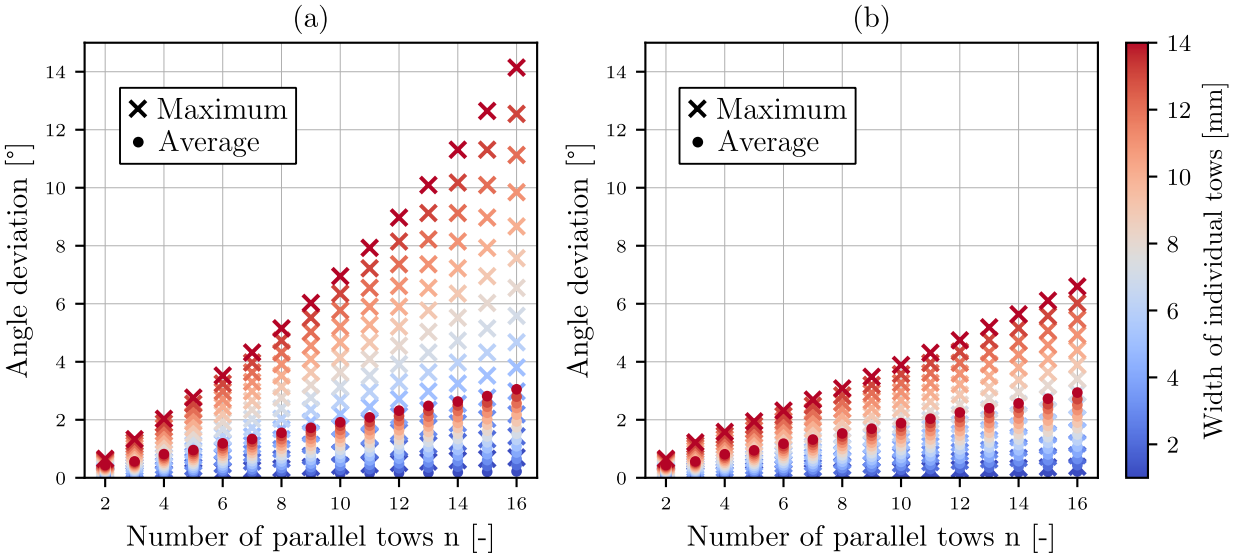

Figure 5: Maximum and average angle deviation for Variable Stiffness Panels with varying number of parallel tows and tape width: (a) One-sided tow cuts, (b) Tow cuts at inside radius

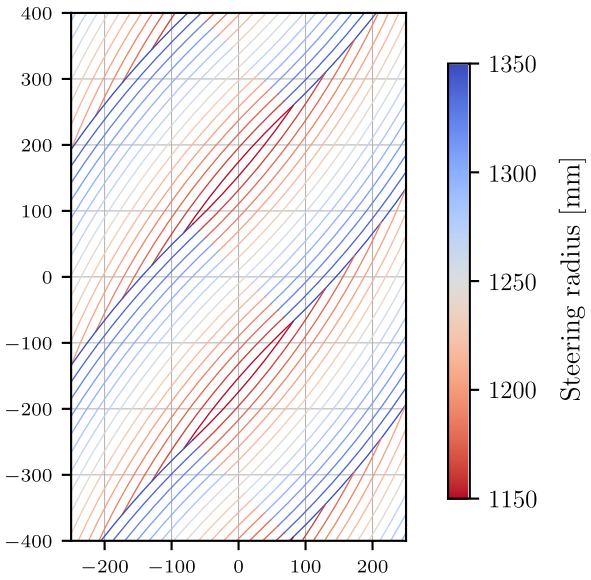

Figure 6: Steering visualization of Variable Stiffness Panels with tow cuts on the inside radius, 14 mm width of individual tows and 16 parallel tows

Steering radii of individual tows for the same example design with 16 parallel tows and 14 mm tape width are presented in Figure 6. There is a direct linear correlation for constant curvature Variable Stiffness Panels between steering radius of the individual tow, the reference curve steering radius and the lateral distance between the respective tow and the reference curve. Figure 7 presents this correlation in a parameter plot. There is a linear increase in the steering radius at the outer edge of the course and a decrease on the inner edge of the course for an increase of both, the number of parallel tows and the width of individual tows, starting from the reference steering radius of 1250 mm. The largest deviation from the reference curve steering radius in positive and negative direction is thus observed for the largest number of parallel tows in combination with the largest width of individual tows.

The gap and overlap defects are also depend on the number of parallel tows and the consolidated tape width. Two example plots of different Variable Stifness Panel configurations with 100 % coverage ratio and the resulting overlap defect pattern are presented in Figure 8. 16 parallel tows in Figure 8(a) result in a significantly lower defect fraction and smaller individual overlap compared to two parallel tows in Figure 8(b).

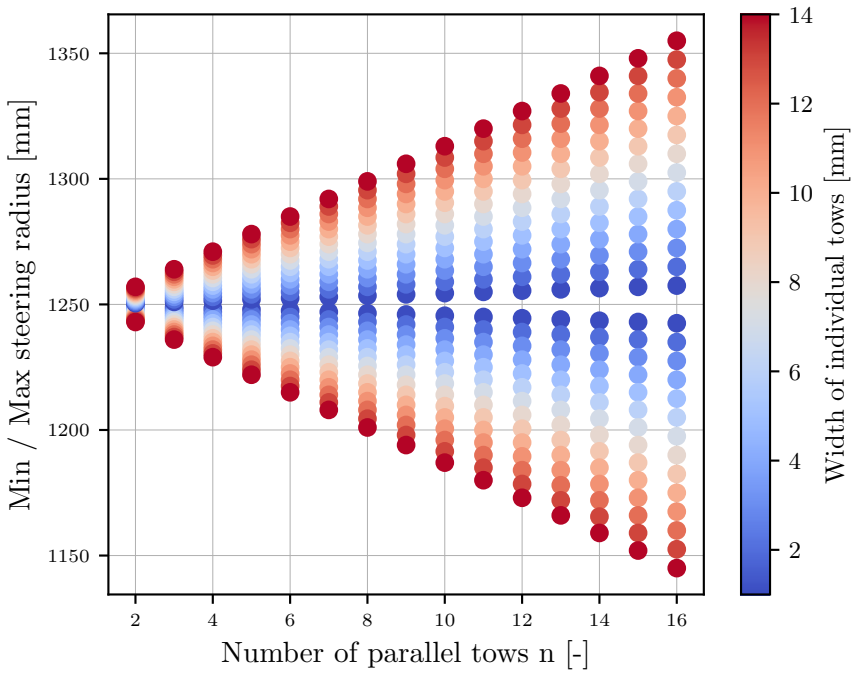

Figure 7: Variable Stiffness Panel analysis of minimum and maximum steering radii of individual tows for varying number of parallel tows and tape width

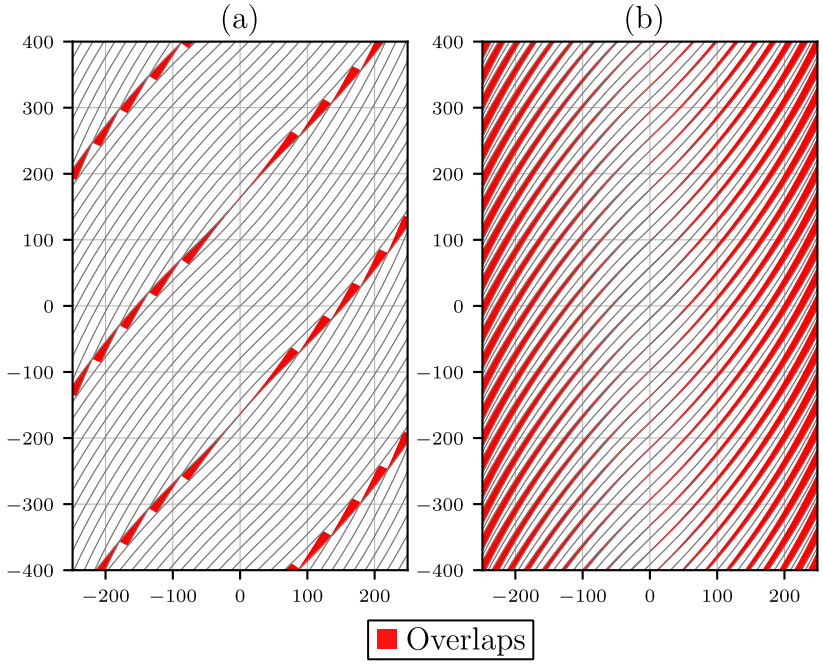

Figure 8: Overlap defect visualization of Variable Stiffness Panels with tow cuts on the inside radius and 14 mm width of individual tows: (a) 16 parallel tows, (b) 2 parallel tows

The corresponding parameter plot (Figure 9) emphasizes that the number of parallel tapes has a major influence, both on the proportion of defects in the total area (Figure 9(a)) and

on the length of the individual defects (Figure 9(b)). For two parallel tows, an overall defect fraction of 22 % and maximum defect length above 500 mm can be observed. In comparison, the width of the individual tows has a significantly lower influence. For 0 % coverage ratio (gap configuration) and one sided tow cuts, the same effect can be observed, as well.

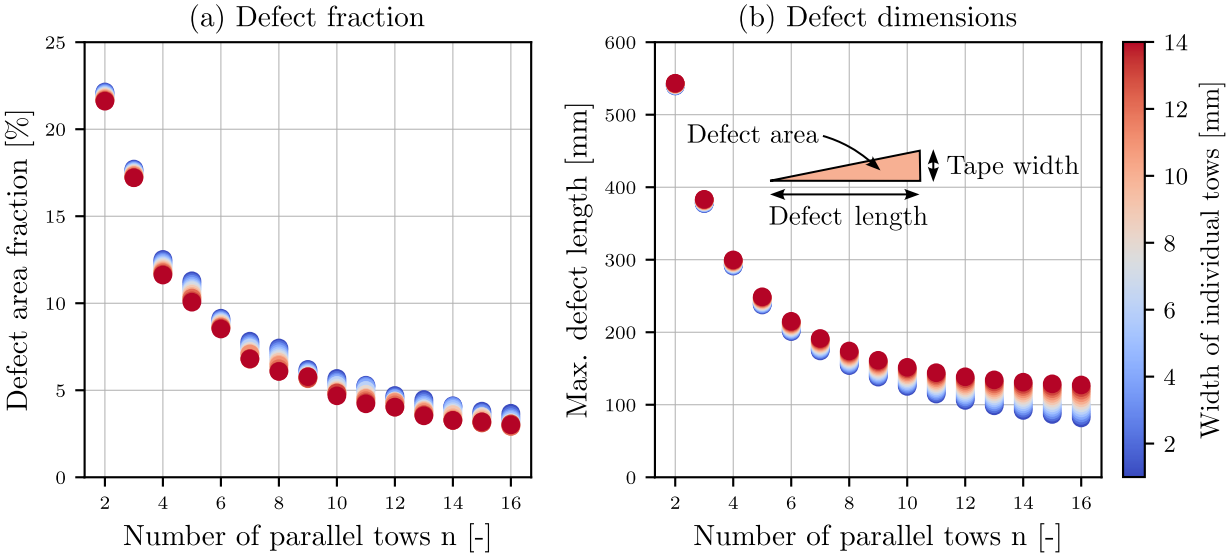

Figure 9: Variable Stiffness Panel defect analysis for varying number of parallel tows and tape width: (a) Area fraction of overlap defects, (b) Maximum length of overlap defects

Gap and overlap defect, however, must be considered not only for one ply, but for the entire laminate. Through thickness staggering of defects is typically employed to reduce the resulting negative effects by distributing the defects throughout the laminate. The gap defects of each subsequent ply should therefore be shifted as far away from the previous ply of the same orientation, as possible. Similar to the shifting of the reference curve to create multiple courses of parallel tows, the staggering is carried out in the same direction as the shifting distance D; in this case the y-direction. The staggering factor is typically expressed as a proportion or multiple of the consolidated tape width. For standard AFP laminates, often a staggering factor of 0.2 to 0.5 is used, in order to avoid super-positioning of tape boundaries of plies of the same orientation. For Variable Stiffness Panels, the position of gap and overlap defects has to be taken into account, as well, to determine the optimum staggering factor. For a Variable Stiffness Panel with multiple Variable stiffness plies of the same orientation, the optimum staggering factor S to achieve the widest possible spacing of the defects can be calculated by dividing the shifting distance D by the number of Variable Stiffness plies of the same orientation. Depending on the number of parallel tows and Variable Stiffness plies of the same orientation, an additional staggering factor has to be added to avoid super-positioning of tape boundaries. Figure 10(a) shows an example plot of staggered overlap defects of a Variable Stiffness Panel with 16 parallel tows, 14 mm width of individual tows and 4 Variable Stiffness plies of the same orientation, which produces the ply stacking sequence $[\langle 23.5|46|23.5\rangle]_4$. The staggering results in an even distribution of the overlap defects throughout the laminate.

The defects are shifted in the y-direction by the staggering factor S. For the example presented, a large distance between the defects is possible. As the ratio of the number of parallel tapes to the tape width decreases, the defects move closer together or can no longer be spatially separated at all. Since, for reasons of symmetry, all effects up to this point could be analyzed using the positive Variable Stiffness orientation, only this side has been considered so far. Realistic Variable Stiffness Panels, however, have a symmetrical stacking sequence. The overlap defect pattern of the corresponding symmetrical laminate is shown in Figure 10(b). The addition of the corresponding mirrored ply to each Variable Stiffness ply results in the ply stacking sequence $[\pm\langle 23.5|46|23.5\rangle]_{2S}$. Inevitably, this results in crossing-points of defects. The sectional views however illustrate, that in most cases there are three or more layers between the superimposed defects. Furthermore many Variable Stiffness Panel designs also contain regular plies with straight layup paths, which can be used to further increase through-thickness separation of defects.

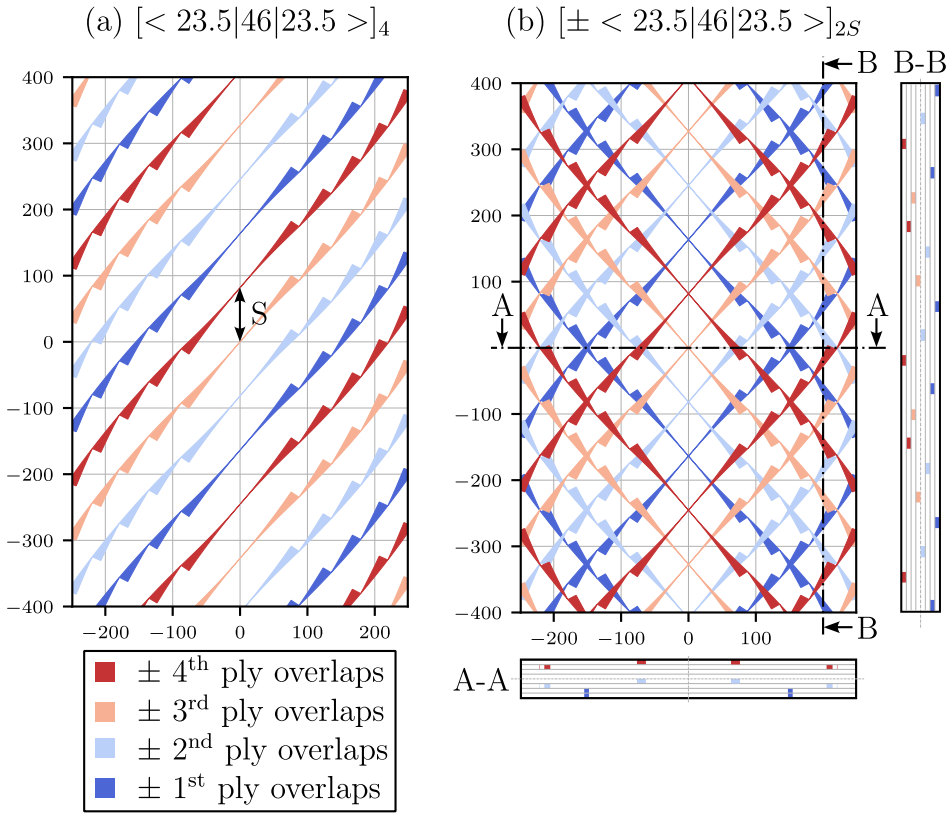

Figure 10: Staggered plies and resulting overlap defect pattern of a Variable Stiffness Panel with 16 parallel tows and 14 mm width of individual tows: (a) Positive ply angle orientation, (b) Positive and negative ply angle orientation and sectional views A-A at y=0 mm and B-B at x=200 mm

There is an infinite number of theoretical parameter combinations for Variable Stiffness Panel design. Usually, however, laminate dimensions and reference curve geometry are predetermined, following stiffness optimization design. For a given set of geometric boundary conditions and stiffness-optimized reference curve, correlations can be derived with regard to the selected AFP layup strategy parameters and the resulting defects. Tow

cuts at the inner radius of a course were identified as a usefull strategy with regard to AFP-manufacturability and limiting angle deviation at the laminate edge regions, compared to one-sided tow cuts, as presented in the literature. Furthermore, using the suggested layup strategy, tape ends with detrimental consolidation quality and layup path deviations due to tape straightening effects can be avoided and minimum cut lengths of AFP end-effectors are not a limiting factor for the manufacturability of the design. Using a larger number of parallel tows results in smaller individual gap or overlap defects and a smaller overall area-related defect fraction. On the other hand, a larger number of parallel tows, particularly in combination with using wider tapes, increases the angle deviation and can decrease the steering radius of the individual tows. The developed Python algorithm can predict exact defect positions and dimensions and can be used as a tool in the decision making process of AFP layup parameter choice.

4. Conclusion

This work introduces a novel layup strategy for constant curvature Variable Stiffness Panels, with tape cuts at the inner radius compared to the literature approach of one-sided tape cuts. This layup strategy considers in-situ AFP manufacturing and avoids tape straightening and sub-optimum consolidation at track ends, as well as minimum cut length capabilities of AFP end effectors. A python based analytical path planning algorithm was developed to generate constant curvature variable Stiffness Panel designs and create layup paths with CAD outputs. This algorithm accurately calculates resulting gap and overlap defects, steering radii and angle deviation and can be used for AFP path planning, prediction of defects, optimizing layup strategies and as a basis for simulation of Variable Stiffness Panels with in-situ AFP manufacturing signature. A comprehensive parameter study found that the suggested novel layup strategy results in lower angle deviation compared to the one-sided tow cuts approach.

Future work will focus on the implementation of steering-induced narrowing effects and arc length dependent onset of steering defects in the Variable Stiffness Panel design. The developed algorithm is used as a basis for currently ongoing Finite Element simulation of Variable Stiffness Panels with in-situ AFP manufacturing signature.

5. Appendix

5.1. Constant Curvature Variable Stiffness Panel Algorithm

A detailed description of the analytical calculations of the constant curvature Variable Stiffness Panel algorithm is presented in this following chapter. Python-based as a Juyter notebooks using the math package for the analytical equations and NumPy, Matplotlib and seaborn for visualization were used for the implementation of the algorithm.

Each set of parallel tapes (course) of the constant curvature Variable Stiffness Panel consists of n parallel tows. The centerline of the center course which leads through the coordinate origin is defined by the reference curve defined in equation 4 determines. The

shifting distance D_0 is then used to create the subsequent course by shifting the reference curves along the y-axis. For a 100 % coverage ratio, D_0 can be calculated as the course width in y-direction at $x = 0$ [11]:

$$D_0 = 2\left(-\sqrt{\left(\rho - \frac{w_c}{2}\right)^2 - (\rho \cdot cos(T_0))^2} + \rho \cdot sin(T_0)\right) \tag{5}$$

where w_c is the course width. The shifting distance $D_{0,gaps}$ is calculated for a 0 % coverage ratio as the course width plus one additional tow of the subsequent course in y-direction at $x = 0$:

$$D_{0,gaps} = D_0 - \sqrt{\left(\rho - \frac{w_c - w_t}{2}\right)^2 - (\rho \cdot cos(T_0))^2} + \rho \cdot sin(T_0) \tag{6}$$

For the subsequent courses, the centerlines can then be calculated using the initial reference curve (Equation 4) and the respective shifting distance. For 100 % coverage ratio:

$$y(x, j) = \begin{cases} \sqrt{\rho^2 - (x - \rho \cdot cos(T_0))^2} - \rho \cdot sin(T_0) + j \cdot D_0 & \text{if } x < 0 \\ -\sqrt{\rho^2 - (x + \rho \cdot cos(T_0))^2} + \rho \cdot sin(T_0) + j \cdot D_0 & \text{if } x \geq 0 \end{cases} \tag{7}$$

and for 0 % overage ratio:

$$y(x, j) = \begin{cases} \sqrt{\rho^2 - (x - \rho \cdot cos(T_0))^2} - \rho \cdot sin(T_0) + j \cdot D_{0,gaps} & \text{if } x < 0 \\ -\sqrt{\rho^2 - (x + \rho \cdot cos(T_0))^2} + \rho \cdot sin(T_0) + j \cdot D_{0,gaps} & \text{if } x \geq 0 \end{cases} \tag{8}$$

where j is an integer variable that is iterated over the number of courses.
Overlaps of subsequentl courses can be avoided via tow cuts at the upper or lower boundary of the course. Fayazbakhsh developed a layup strategy with one sided tow cuts at the upper course boundary [11]. Tow cut positions can be determined as the intersections between the lower boundary of the subsequent course and the tows of the center course. The parallel layup of the tows in a course results in a shift of the inflection point of the tows in comparison to the reference curve. The case differentiation of the parallel shifted curve functions requires the x-coordinate of the inflection point. The x-coordinate of the inflection point can be calculated for the lower boundary of all courses as:

$$B_0 = \frac{1}{2} \cdot w_c \cdot cos(T_0) \tag{9}$$

The same x-coordinate applies for all coverage ratios. For 100 % coverage ratio, the lower boundary curves of the courses can then be calculated as:

$$y_{bottom,overlaps}(x, j) = \begin{cases} \sqrt{(\rho - \frac{w_c}{2})^2 - (x - \rho \cdot cos(T_0))^2} - \rho \cdot sin(T_0) + j \cdot D_0 & \text{if } x \leq B_0 \\ -\sqrt{(\rho + \frac{w_c}{2})^2 - (x + \rho \cdot cos(T_0))^2} + \rho \cdot sin(T_0) + j \cdot D_0 & \text{if } x > B_0 \end{cases} \tag{10}$$

For 0 % coverage ratio the lower boundary curves can be calculated using the shifting distance $D_{0,gaps}$:

$$y_{bottom,gaps}(x, j) = \begin{cases} \sqrt{(\rho - \frac{w_c}{2})^2 - (x - \rho \cdot cos(T_0))^2} - \rho \cdot sin(T_0) + j \cdot D_{0,gaps} & \text{if } x \leq B_0 \\ -\sqrt{(\rho + \frac{w_c}{2})^2 - (x + \rho \cdot cos(T_0))^2} + \rho \cdot sin(T_0) + j \cdot D_{0,gaps} & \text{if } x > B_0 \end{cases} \tag{11}$$

For 100 % coverage ratio layup, the tow cuts can be calculated as the intersection between the lower course boundary curve of the course above the main course and the lower boundaries of the individual tows of the main course. To this end, the x-coordinate of the inflection point of the individual tows is calculated as:

$$B(i) = w_c \cdot (\frac{1}{2} - \frac{i}{n}) \cdot w_c \cdot cos(T_0) \tag{12}$$

where i is an integer variable that is iterated over the number of tows and n is the total number of parallel tows of each course. The lower boundaries of the individual tows are defined as:

$$y_{tows,bottom}(x,i) = \begin{cases} \sqrt{(\rho - \frac{w_c}{2} + i \cdot w_t)^2 - (x - \rho \cdot cos(T_0))^2} - \rho \cdot sin(T_0) + j \cdot D_{0,gaps} \\ \text{if } x \leq B(i) \\ -\sqrt{(\rho + \frac{w_c}{2} - i \cdot w_t)^2 - (x + \rho \cdot cos(T_0))^2} + \rho \cdot sin(T_0) + j \cdot D_{0,gaps} \\ \text{if } x > B(i) \end{cases} \tag{13}$$

Equating the functions of the lower tow boundaries of the main course and the lower course boundary curve of the course above the main course produces the intersection points that define the tow cut locations.

$$x_{intersect,overlaps}(i) = \begin{cases} (D_0 \cdot \rho \cdot cos(T_0) - \frac{1}{4} \cdot (-(-2D_0 + i \cdot w_t + w_t) \cdot (2D_0 + i \cdot w_t + w_t) \cdot \\ (-2D_0 - w_c + i \cdot w_t + 2\rho + w_t) \cdot (2D_0 - w_c + i \cdot w_t + 2\rho + w_t))^{\frac{1}{2}}/D_0 \\ \text{if } B(i) \leq 0 \\ (-D_0 \cdot \rho \cdot cos(T_0) + \frac{1}{4} \cdot ((-2D_0 + i \cdot w_t + w_t) \cdot (2D_0 + i \cdot w_t + w_t) \cdot \\ (2D_0 - w_c + i \cdot w_t - 2\rho + w_t) \cdot (2D_0 + w_c - i \cdot w_t + 2\rho - w_t))^{\frac{1}{2}})/D_0) \\ \text{if } B(i) > 0 \end{cases} \tag{14}$$

Similarly equating the lower course boundary curve of the course above the main course and the upper boundaries of the individual tows of the main course produces the intersection points which define the tow cut locations for the tow cuts of 0 % coverage ratio layup.

$$x_{intersect,gaps}(i) = \begin{cases} \rho \cdot (D_0^2 + 2D_0 \cdot D_{0,gaps} + D_{0,gaps}^2) \cdot cos(T_0) - \frac{1}{2} \cdot (-(D_0 + D_{0,gaps} - i \cdot w_t - w_t) \cdot \\ (D_0 + D_{0,gaps} + i \cdot w_t + w_t) \cdot (D_0 + D_{0,gaps} - w_c + i \cdot w_t + 2\rho + w_t) \cdot \\ (D_0 + D_{0,gaps} + w_c - i \cdot w_t - 2\rho - w_t))^{\frac{1}{2}} \cdot \\ (D_0 + D_{0,gaps}))/(D_0^2 + 2D_0 \cdot D_{0,gaps} + D_{0,gaps}^2 \\ \text{if } B(i) \leq 0 \\ (-\rho \cdot (D_0^2 + 2D_0 \cdot D_{0,gaps} + D_{0,gaps}^2) \cdot cos(T_0) + \frac{1}{2} \cdot (-(D_0 + D_{0,gaps} - i \cdot w_t - w_t) \cdot \\ (D_0 + D_{0,gaps} + i \cdot w_t + w_t) \cdot (D_0 + D_{0,gaps} - w_c + i \cdot w_t - 2\rho + w_t) \cdot \\ (D_0 + D_{0,gaps} + w_c - i \cdot w_t + 2\rho - w_t))^{\frac{1}{2}} \cdot \\ (D_0 + D_{0,gaps}))/(D_0^2 + 2D_0 \cdot D_{0,gaps} + D_{0,gaps}^2 \\ \text{if } B(i) > 0 \end{cases} \tag{15}$$

The corresponding y-coordinates can be calculated by inserting the $x_{intersect,overlaps}(i)$ and $x_{intersect,gaps}(i)$ into the lower course boundary curve for the respective coverage ratio. the intersection points and resulting tow cuts for 100 % coverage ratio and 0 % coverage ratio are shown in Figure 11(b) and (c), respectively.

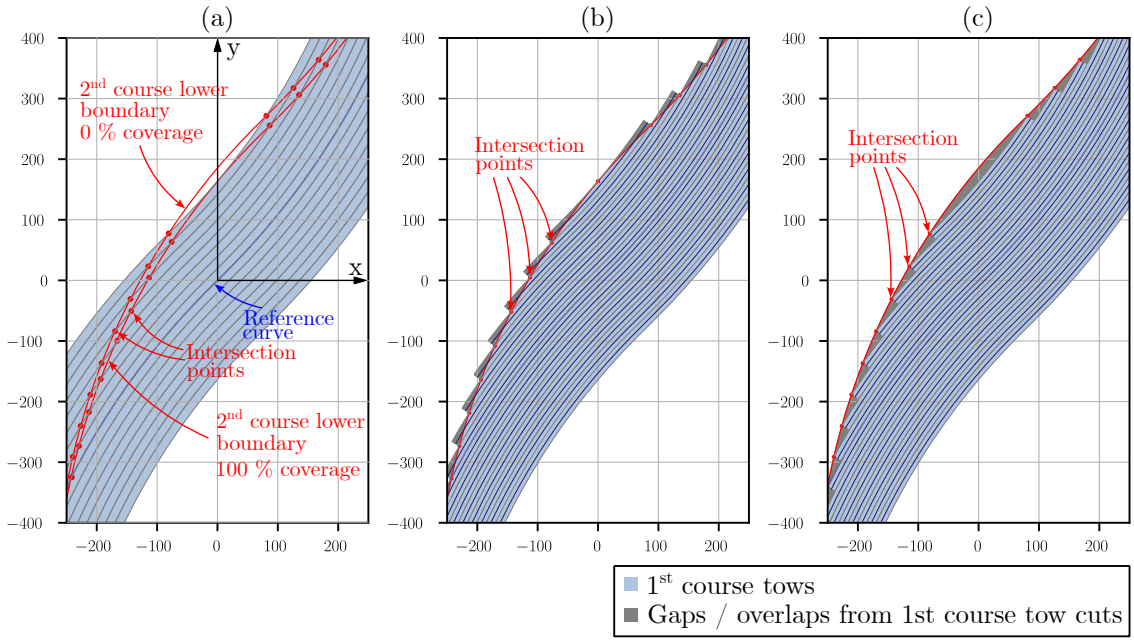

Figure 11: Constant curvature Variable Stiffness Panel design with one-sided tow cuts: (a) definition of intersection points, (b) 100 % coverage ratio tow cuts, (c) 0 % coverage ratio tow cuts

For the novel approach presented in this work, which uses tows only on the inside radius of the steered course, adjustments are required to the layup strategy introduced above. For the reference curve with the present orientation, tows are cut at the lower boundary of the course for $x \leq 0$ and at the upper boundary of the course for $x > 0$. The lower course boundary curve of the course above the main course is thus used for tow cut definition as in the one-sided tow cut strategy for $x > 0$. For $x \leq 0$ on the other hand, the upper course boundary curve of the course below the main course is used to determine the intersection points.

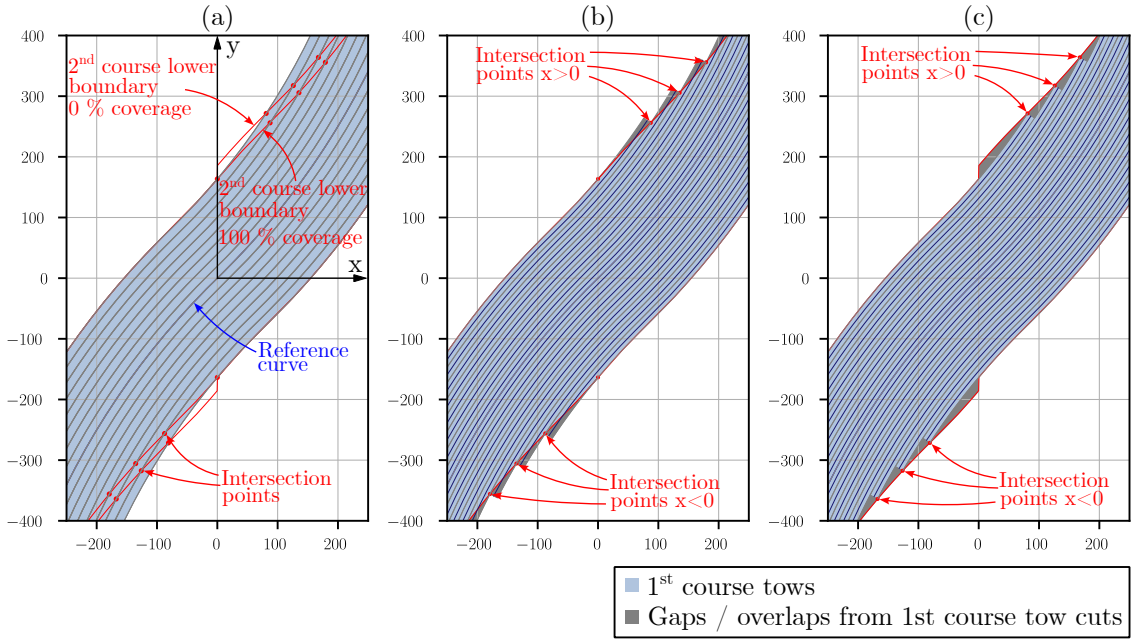

Figure 12: Constant curvature Variable Stiffness Panel design with tow cuts at the inner radius: (a) definition of intersection points, (b) 100 % coverage ratio tow cuts, (c) 0 % coverage ratio tow cuts

The upper course boundary curves for 100 % coverage ratio can be calculated in a similar way to the bottom boundary curves:

$$y_{upper,overlaps}(x,j) = \begin{cases} \sqrt{(\rho + \frac{w_c}{2})^2 - (x - \rho \cdot cos(T_0))^2} - \rho \cdot sin(T_0) + j \cdot D_0 & \text{if } x \leq -B_0 \\ -\sqrt{(\rho - \frac{w_c}{2})^2 - (x + \rho \cdot cos(T_0))^2} + \rho \cdot sin(T_0) + j \cdot D_0 & \text{if } x > -B_0 \end{cases} \tag{16}$$

For 0 % coverage ratio the upper course boundary curves can be determined following:

$$y_{upper,gaps}(x,j) = \begin{cases} \sqrt{(\rho + \frac{w_c}{2})^2 - (x - \rho \cdot cos(T_0))^2} - \rho \cdot sin(T_0) + j \cdot D_{0,gaps} & \text{if } x \leq -B_0 \\ -\sqrt{(\rho - \frac{w_c}{2})^2 - (x + \rho \cdot cos(T_0))^2} + \rho \cdot sin(T_0) + j \cdot D_{0,gaps} & \text{if } x > -B_0 \end{cases} \tag{17}$$

The intersection points for tow cut positions for $x \leq 0$, can by calculated by equating $y_{upper,overlaps}(x,j)$ and $y_{upper,gaps}(x,j)$ with $y_{tows,bottom}(x,i)$ and $y_{tows_upper}(x,i)$ for 0 % and 100 % coverage ratio, respectively. Accordingly, for $x > 0$, intersection points for tow cut positions are determined by equating $y_{bottom,overlaps}(x,j)$ and $y_{bottom,gaps}(x,j)$ with $y_{tows,bottom}(x,i)$ and $y_{tows_upper}(x,i)$ for 0 % and 100 % coverage ratio, respectively. Figure 12(a) shows the resulting boundary curves and intersection point. The resulting tow cuts and defects are shown in Figure 12(b) and (c), for 0 % and 100 % coverage ratio, respectively. A symmetrical Variable Stiffness Panel design is created by adding mirrored

plies. To this end, for the presented reference curve and path propagation strategy, the paths are mirrored on the y-axis. Shifted reference curves for the mirrored ply orientation are presented in Figure 13(a). Figure 13(a) and (b) show resulting defect patterns for 100 % coverage ratio and one-sided tow cuts and tow cuts at the inner radius, respectively.

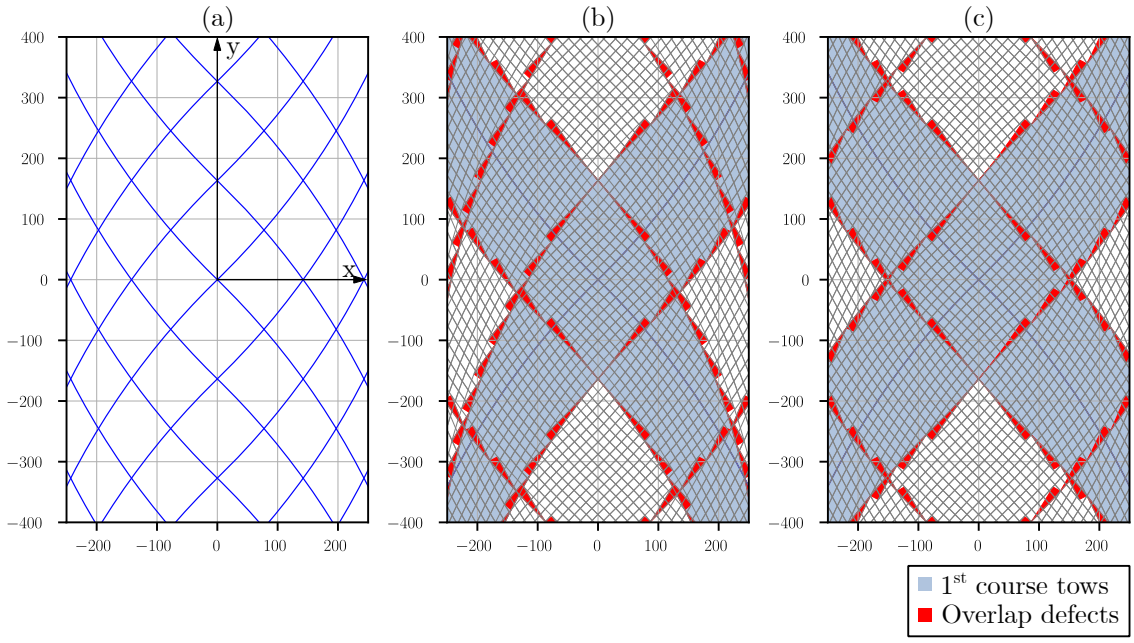

Figure 13: Mirrored constant curvature Variable Stiffness plies: (a) Mirrored reference curves, (b) One-sided tow cuts and 100 % coverage ratio, (c) tow cuts at the inner radius and 100 % coverage ratio tow cuts

The symmetrical laminate structure leads to equivalent defects in both orientations. The defect geometries can thus be determined for one direction only. The analytical path planning functions can be used to calculate the exact magnitudes of the three primary defect types, steering radius and arc length, gap or overlap defects and angle deviation. Arc lengths of steered layup paths are calculated from the tow-cut positions, inflection points, ply boundaries and steering radii of individual tows (Figure 14(a)). The curvature direction changes at the inflection point of each individual tow. Gap or overlap defect areas can be calculated from the difference of the integrals of the upper and lower defects boundary over the length in x-direction of each individual defect. The length of each individual gap or overlap defect is calculated using the euclidean distance along the major cathetus of the triangluar defect. The width of each defect is assumed as the consolidated tape width (Figure 14(b).

The local angle deviation θ_{dev} can be calculated at each x-position as the difference between the derivatives of the respective tow center curve and the reference curve:

$$\theta_{dev}(x,i) = \arctan\left(\frac{dy_{tows}(x,i)}{dx}\right) - \arctan\left(\frac{dy(x)}{dx}\right) \tag{18}$$

For the current example with 100 % coverage ratio and tow cuts at the inner radius, the angular deviation is shown in Figure 14(c).

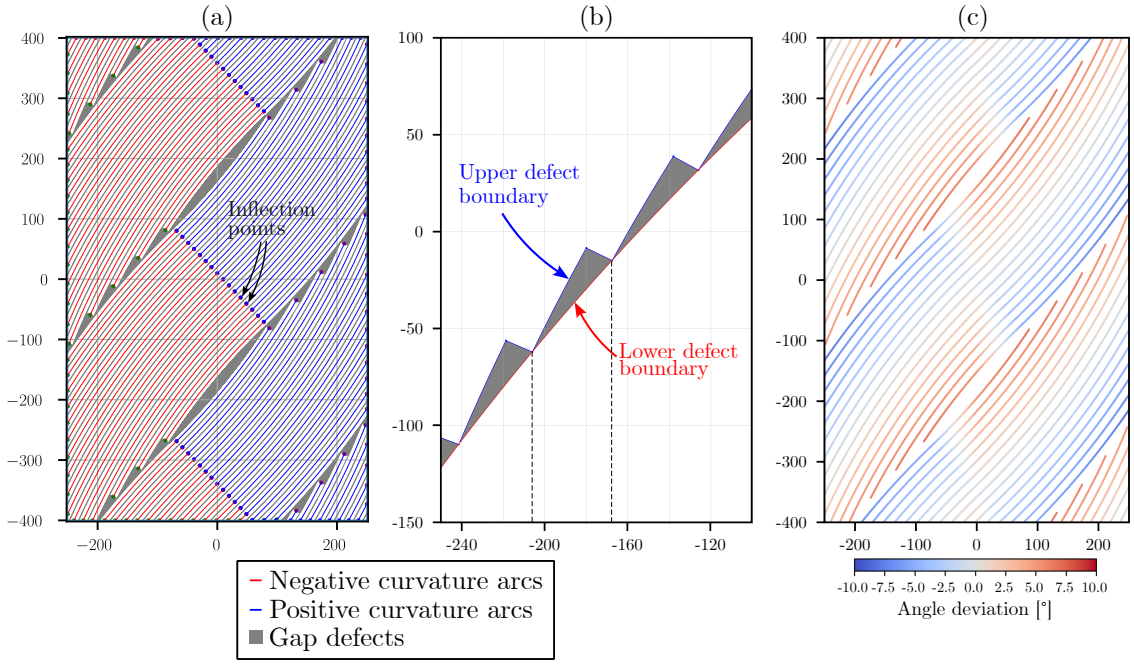

Figure 14: Variable Stiffness defect analysis: (a) Steering arc length analysis, (b) Defect area analysis, (c) Angle deviation analysis

6. References

[1] A. H. Akbarzadeh, M. Arian Nik, and D. Pasini. "The role of shear deformation in laminated plates with curvilinear fiber paths and embedded defects". English. In: *Composite Structures* 118 (Dec. 2014), 217–227. ISSN: 0263-8223. DOI: {10.1016/j.compstruct.2014.07.027}.

[2] Ahmad Alhajahmad, Mostafa M. Abdalla, and Zafer Gürdal. "Optimal Design of Tow-Placed Fuselage Panels for Maximum Strength with Buckling Considerations". In: *Journal of Aircraft* 47.3 (May 2010), pp. 775–782. DOI: 10.2514/1.40357.

[3] Adriana Blom, Patrick Stickler, and Zafer Gurdal. "Design and Manufacture of a Variable-Stiffness Cylindrical Shell". In: *Proceedings of the SAMPE Europe 30th International Conference*. Jan. 2009.

[4] Adriana W. Blom, Mostafa M. Abdalla, and Zafer Gurdal. "Optimization of course locations in fiber-placed panels for general fiber angle distributions". English. In: *Composites Science and Technology* 70.4 (Apr. 2010), pp. 564–570. ISSN: 0266-3538. DOI: {10.1016/j.compscitech.2009.12.003}.

[5] Adriana W. Blom, Patrick B. Stickler, and Zafer Gürdal. "Optimization of a composite cylinder under bending by tailoring stiffness properties in circumferential direction". In: *Composites Part B: Engineering* 41.2 (2010), pp. 157–165. ISSN: 1359-8368. DOI: https://doi.org/10.1016/j.compositesb.2009.10.

004. URL: https://www.sciencedirect.com/science/article/pii/S1359836809001887.

[6] Adriana W. Blom et al. "A Theoretical Model to Study the Influence of Tow-drop Areas on the Stiffness and Strength of Variable-stiffness Laminates". English. In: *Journal of Composite Materials* 43.5 (Mar. 2009). 22nd Annual Technical Conference of the American-Society-for-Composites, Seattle, WA, SEP 17-19, 2007, 403–425. ISSN: 0021-9983. DOI: {10.1177/0021998308097675}.

[7] Adriana W. Blom et al. "Fiber path definitions for elastically tailored conical shells". In: *Composites Part B: Engineering* 40.1 (Jan. 2009), pp. 77–84. DOI: 10.1016/j.compositesb.2008.03.011.

[8] Hendrik Brandis. "Konzeption eines integrierten Tape-Legesystems für die Applikation nichtabwickelbarer Luftfahrzeugstrukturen aus faserverstärktem Kunststoff". PhD thesis. Technischen Universität München, July 1991.

[9] Gearóid J. Clancy, Ronan O'Higgins, and Paul M. Weaver. "Spreading of Carbon Fiber/Thermoplastic Pre-preg Tapes". In: *AIAA Scitech 2020 Forum*. 2020, p. 0481.

[10] O. Falcó et al. "Variable-stiffness composite panels: As-manufactured modeling and its influence on the failure behavior". In: *Composites Part B: Engineering* 56 (2014), pp. 660–669. ISSN: 1359-8368. DOI: https://doi.org/10.1016/j.compositesb.2013.09.003. URL: https://www.sciencedirect.com/science/article/pii/S1359836813005167.

[11] Kazem Fayazbakhsh. "The impact of gaps and overlaps on variable stiffness composites manufactured by Automated Fiber Placement". PhD thesis. Department of Mechanical EngineeringMcGill University, Montreal, 2013.

[12] Kazem Fayazbakhsh et al. "Defect layer method to capture effect of gaps and overlaps in variable stiffness laminates made by Automated Fiber Placement". In: *Composite Structures* 97 (2013), pp. 245–251. ISSN: 0263-8223. DOI: https://doi.org/10.1016/j.compstruct.2012.10.031. URL: http://www.sciencedirect.com/science/article/pii/S0263822312005272.

[13] Hossein Ghiasi et al. "Optimum stacking sequence design of composite materials Part II: Variable stiffness design". In: *Composite Structures* 93.1 (2010), pp. 1–13. ISSN: 0263-8223. DOI: https://doi.org/10.1016/j.compstruct.2010.06.001. URL: https://www.sciencedirect.com/science/article/pii/S0263822310001947.

[14] Z. Gurdal and R. Olmedo. "In-plane response of laminates with spatially varying fiber orientations - Variable stiffness concept". English. In: *AIAA JOURNAL* 31.4 (1993), 751–758. ISSN: 0001-1452. DOI: {10.2514/3.11613}.

[15] Zafer Gurdal, Brian Tatting, and K Wu. "Tow-placement technology and fabrication issues for laminated composite structures". In: *46th AIAA/ASME/ASCE/AHS/ASC structures, structural dynamics and materials conference*. 2005.

[16] Z. Gürdal, B. F. Tatting, and C. K. Wu. "Variable stiffness composite panels: Effects of stiffness variation on the in-plane and buckling response". In: *Composites Part A: Applied Science and Manufacturing* 39.5 (2008), pp. 911–922. ISSN: 1359-835X. DOI: https://doi.org/10.1016/j.compositesa.2007.11.015. URL: https://www.sciencedirect.com/science/article/pii/S1359835X07002643.

[17] Zhi Hong, Daniel Peeters, and Sergio Turteltaub. "An enhanced curvature-constrained design method for manufacturable variable stiffness composite laminates". English. In: *Computers & Structures* 238 (Oct. 2020). ISSN: 0045-7949. DOI: {10.1016/j.compstruc.2020.106284}.

[18] Guanxin Huang, Hu Wang, and Guangyao Li. "An efficient reanalysis assisted optimization for variable-stiffness composite design by using path functions". English. In: *Composite Structures* 153 (Oct. 2016), 409–420. ISSN: 0263-8223. DOI: {10.1016/j.compstruct.2016.06.043}.

[19] A. Khani et al. "Design, manufacturing and testing of a fibre steered panel with a large cut-out". English. In: *Composite Structures* 180 (Nov. 2017), pp. 821–830. ISSN: 0263-8223. DOI: {10.1016/j.compstruct.2017.07.086}.

[20] B. C. Kim et al. "Limitations of fibre placement techniques for variable angle tow composites and their process-induced defects". In: *Proceedings of the 18th International Conference on Composite Materials (ICMM18), Jeju, Korea*. 2010, pp. 21–26.

[21] C. S. Lopes, Z. Gürdal, and P. P. Camanho. "Tailoring for strength of composite steered-fibre panels with cutouts". In: *Composites Part A: Applied Science and Manufacturing* 41.12 (Dec. 2010), pp. 1760–1767. DOI: 10.1016/j.compositesa.2010.08.011.

[22] C. S. Lopes et al. "Progressive failure analysis of tow-placed, variable-stiffness composite panels". English. In: *International Journal of Solids and Structures* 44.25-26 (Dec. 2007), pp. 8493–8516. ISSN: 0020-7683. DOI: {10.1016/j.ijsolstr.2007.06.029}.

[23] Cláudio S. Lopes, Joris J.C. Remmers, and Zafer Gürdal. "Influence of Porosity on the Interlaminar Shear Strength of Fibre-Metal Laminates". In: *Key Engineering Materials* 383 (Nov. 2008), pp. 35–52. DOI: 10.4028/www.scientific.net/KEM.383.35.

[24] G. Gonzalez Lozano, A. Tiwari, and C. Turner. "A design algorithm to model fibre paths for manufacturing of structurally optimised composite laminates". English. In: *Composite Structures* 204 (Nov. 2018), 882–895. ISSN: 0263-8223. DOI: {10.1016/j.compstruct.2018.07.088}.

[25] A. Marouene et al. "Buckling behavior of variable-stiffness composite laminates manufactured by the tow-drop method". In: *Composite Structures* 139 (2016), pp. 243–253. ISSN: 0263-8223. DOI: https://doi.org/10.1016/j.compstruct.2015.12.025. URL: https://www.sciencedirect.com/science/article/pii/S0263822315011150.

[26] A. Marouene et al. “Effects of gaps and overlaps on the buckling behavior of an optimally designed variable-stiffness composite laminates - A numerical and experimental study”. English. In: *Composite Structures* 140 (Apr. 2016), 556–566. ISSN: 0263-8223. DOI: {10.1016/j.compstruct.2016.01.012}.

[27] Vibhas Mishra, Daniel M. J. Peeters, and Mostafa M. Abdalla. “Stiffness and buckling analysis of variable stiffness laminates including the effect of automated fibre placement defects”. English. In: *Composite Structures* 226 (Oct. 2019). ISSN: 0263-8223. DOI: https://doi.org/10.1016/j.compstruct.2019.111233.

[28] Yuto Mori, Ryosuke Matsuzaki, and Naoya Kumekawa. “Variable thickness design for composite materials using curvilinear fiber paths”. In: *Composite Structures* 263 (2021), p. 113723. ISSN: 0263-8223. DOI: https://doi.org/10.1016/j.compstruct.2021.113723. URL: https://www.sciencedirect.com/science/article/pii/S0263822321001847.

[29] Mahdi Arian Nik et al. “Optimization of variable stiffness composites with embedded defects induced by Automated Fiber Placement”. English. In: *Composite Structures* 107 (Jan. 2014), 160–166. ISSN: 0263-8223. DOI: {10.1016/j.compstruct.2013.07.059}.

[30] Daniel M. J. Peeters, Gustavo Gonzalez Lozano, and Mostafa M. Abdalla. “Effect of steering limit constraints on the performance of variable stiffness laminates”. English. In: *Computers and Structures* 196 (Feb. 2017), 94–111. ISSN: 0045-7949. DOI: {10.1016/j.compstruc.2017.11.002}.

[31] Daniel M. J. Peeters et al. “Optimal design, manufacturing and testing of non-conventional laminates”. English. In: *Composite Structures* 210 (Feb. 2019), 29–40. ISSN: 0263-8223. DOI: {10.1016/j.compstruct.2018.10.062}.

[32] Lukas Raps, Ashley R. Chadwick, and Heinz F. Voggenreiter. “Effect of geometry-induced triangular gap and overlap defects on in-situ AFP-manufactured structures”. In: *Composite Structures* 373 (2025), p. 119556. ISSN: 0263-8223. DOI: https://doi.org/10.1016/j.compstruct.2025.119556. URL: https://www.sciencedirect.com/science/article/pii/S0263822325007214.

[33] Pedro Ribeiro et al. “A review on the mechanical behaviour of curvilinear fibre composite laminated panels”. In: *Journal of Composite Materials* 48.22 (2014), pp. 2761–2777. DOI: 10.1177/0021998313502066. eprint: https://doi.org/10.1177/0021998313502066. URL: https://doi.org/10.1177/0021998313502066.

[34] Guillaume Rousseau et al. “Automated Fiber Placement Path Planning: A state-of-the-art review”. In: *Computer-Aided Design and Applications* 16.2 (2019), pp. 172–203.

[35] Brian Tatting, Tafer Gürdal, and Dawn Jegley. *Design and Manufacture of Elastically TailoredTow Placed Plates*. Tech. rep. ADOPTECH, Inc., Blacksburg, Virginia, 2002.

[36] Avinkrishnan A. Vijayachandran and Anthony M. Waas. “Minimizing stress concentrations using steered fiberpaths and incorporating realistic manufacturing signatures”. In: *International Journal of Non-Linear Mechanics* 146 (2022), p. 104160. ISSN: 0020-7462. DOI: https://doi.org/10.1016/j.ijnonlinmec.2022.104160. URL: https://www.sciencedirect.com/science/article/pii/S0020746222001585.

[37] K. Wu et al. “Design and Manufacturing of Tow-Steered Composite Shells Using Fiber Placement”. In: *50th AIAA/ASME/ASCE/AHS/ASC Structures, Structural Dynamics, and Materials Conference*. 2012. DOI: 10.2514/6.2009-2700. eprint: https://arc.aiaa.org/doi/pdf/10.2514/6.2009-2700. URL: https://arc.aiaa.org/doi/abs/10.2514/6.2009-2700.

[38] Qi Xia and Tielin Shi. “Optimization of composite structures with continuous spatial variation of fiber angle through Shepard interpolation”. English. In: *Composite Structures* 182 (Dec. 2017), 273–282. ISSN: 0263-8223. DOI: {10.1016/j.compstruct.2017.09.052}.

[39] Z. Zheng et al. “Failure analysis of variable-stiffness laminate considering manufacturing defects”. English. In: *2nd international Workshop on Materials Science and Mechanical Engineering (IWMSME2018)*. Ed. by Fan, HJ. Vol. 504. IOP PUBLISHING LTD, 2018. DOI: {10.1088/1757-899X/504/1/012055}.

[40] Yingdan Zhu et al. “Fiber path optimization based on a family of curves in composite laminate with a center hole”. English. In: *Composites Part B: Engineering* 111 (Feb. 2017), 91–102. ISSN: 1359-8368. DOI: {10.1016/j.compositesb.2016.11.051}.